Journal of Solid Mechanics Vol. 3, No. 2 (2011) pp. 132-141

Thermal Stress Analysis of a Composite Cylinder Reinforced with FG SWCNTs

A. Ghorbanpour Arani[1,2,*], S. Amir[1], V. Sadooghi[1], M. Mohammadimehr[1]

[1] *Department of Mechanical Engineering, Faculty of Engineering, University of Kashan, Kashan, Islamic Republic of Iran*
[2] *Institute of Nanoscience & Nanotechnology, University of Kashan, Kashan, Islamic Republic of Iran*

Received 26 April 2011; accepted 16 June 2011

ABSTRACT

Thermal stress analysis of a thick-walled cylinder reinforced with functionally graded (FG) single-walled carbon nanotubes (SWCNTs) is considered in radial direction. Thick-walled cylinder is subjected to a thermal field. Two layouts of variations in the volume fraction of SWCNTs were considered in the composite cylinder along the radius from inner to outer surface, where their names are incrementally decreasing (Inc Dec) and incrementally increasing (Inc Inc). Micromechanical models based on the Mori-Tanaka is used to define effective macroscopic properties of the nano composite shell. Using equations of motion, stress-strain and their corresponding constitutive correlations of a polystyrene vessel, a second order ordinary differential equation was proposed based on the radial displacement. The higher order governing equation was solved in order to obtain the distribution of displacement and thermal stresses in radial, circumferential and axial directions. The results indicate that FG distributions of SWCNTs have significant effect on thermal stresses and displacements in axial, radial and circumferential directions, so that in Inc Inc layout, the radial and circumferential stresses are lower than of other FG structures.

Keywords: Thermal Stress analysis; Nano Composite; Mori-Tanaka; FG SWCNTs reinforcement; Thick-walled cylinder.

1 INTRODUCTION

CARBON nanotubes (CNTs) with high aspect ratio, large surface area, low density as well as excellent mechanical, electrical and thermal properties have attracted scientific and technological interests globally [1-2]. These properties have inspired interest in using CNTs as reinforcing materials for polymer- matrix, metal- matrix or ceramic-matrix composites to obtain light-weight structural materials with enhanced mechanical, electrical and thermal properties. Therefore, the presence of the nanotubes can improve the strength and stiffness of polymers as well as electrical and thermal conductivities to polymer based composite systems [3-7]. Evidently, such composites are of paramount interest in aeronautic and astronautic technology, automobile and many other modern industries.

Considering nanocomposite applications in actual structures, Qian et al. [8] reported a MWCNTs reinforced by polystyrene with good dispersion and CNT-matrix adhesion. They achieved improvements of 40% in the elastic modulus and 25% in the tensile strength by adding only 0.5% CNT. Odergart et al. [9] presented techniques to evaluate elastic properties of nanocomposites and found that adding volume fraction by 1% yielded a maximum stiffness for CNT length of 60-80 nm for both aligned and random orientations. Wuite and Adali [10] examined deflection and stress of nanocomposite reinforced beams and reported significant improvement in beam stiffness.

* Corresponding author. Tel.: +98 913 162 6594 ; Fax: +98 361 5912424.
E-mail address: aghorban@kashanu.ac.ir (A. Ghorbanpour Arani).

Bending and local buckling of a nanocomposite beam reinforced by a SWCNT was also studied by Vodenitcharova and Zhang [11]. Studies conducted by Han and Elliot [12] and Zhu et al. [13] on simulation of the elastic properties of polymer/CNT composites and stress-strain curves for CNT reinforced Epon 862 composites, respectively, suggested that addition of a small amount of CNT improved mechanical, electrical and thermal properties of polymeric composites. Their useful results can be applied to the global response of CNT reinforced with composites in an actual structural element.

Functionally graded materials (FGMs) are a new generation of composites in which the microstructural details are spatially varied through non-uniform distribution of the reinforcement phase in order to improve properties such as linear and nonlinear bending behaviors, and interfacial bonding strength. Shen [14] studied these for the plates at various thermal environments, while Ke et al. [15] examined nonlinear free-vibration of FGM carbon nanotube reinforced composites for beams. As far as work on cylinder is concerned which extensive workers have been carried out due to industrial interests hallow cylinders for analysis of thermally excited responses to elastic bodies [16-17]. Ding et al. [18] studied a theoretical solution of cylindrically isotropic cylindrical tube for the axisymmetric plane strain dynamic thermoelastic problem. For pyroelectric material, Pelletier and Vel [19] presented an exact solution for the steady-state thermoelastic response of functionally graded orthotropic cylindrical shells. As for non-homogeneity of materials, the special case where the Young's modulus has a power law dependence on the radial coordinate, with the linear thermal expansion coefficient and the constant Poisson's ratio has been studied by many workers [20-21]. Abd-Alla and Farhan [22] analyzed the effect of the non-homogenity on the composite infinite cylinder of orthotropic material.

Motivated by these considerations, the need for the investigation of a FG material is applied to the nanocomposite cylinder reinforced by SWCNTs which material properties of SWCNTs are assumed to be temperature, is very much felt. The material properties of functionally graded CNTs are assumed to be graded in radial direction. The cylinder is subjected to a steady state thermal field. The material properties of FG SWCNTs are obtained using the Mori-Tanaka model. Using equations of motion, stress-strain and their corresponding constitutive correlations of a polystyrene vessel, a second order ordinary differential equation is proposed based on the radial displacement which is solved in order to obtain the distribution of radial, circumferential and axial stresses.

2 GOVERNING EQUATIONS

In this work, Mori-Tanaka micromechanical model was used to determine the effective material properties of the SWCNTs reinforced by polystyrene nanocomposite due to its simplicity and accuracy at high volume fraction of CNTs inclusions [23]. Similar to [23] a representative volume element (RVE) V for the composite is illustrated in Fig. 1, in which a linear elastic polymer matrix is reinforced by a SWCNT that is aligned, straight and infinite in length in x_2 direction.

The RVE boundary of δV is also subjected either to tractions corresponding to a uniform overall stress σ^0 or to displacements compatible to a prescribed uniform overall strain ε_0 and the method assumes that each inclusion is embedded in an infinite pristine matrix subjected to an effective average stress σ_m or an effective average strain ε_m in the far field [8]. The matrix is also assumed to be elastic and isotropic. Each straight CNT is modeled as a long fiber with transversely isotropic elastic properties. Therefore, the composite too, is transversely isotropic; its constitutive relation $\sigma = C : \varepsilon$ can be expressed as [23]:

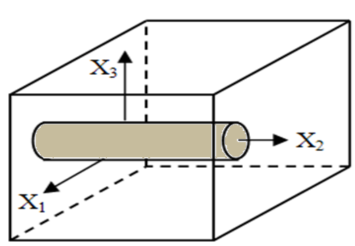

Fig. 1
Schematic of RVE of a composite reinforced with CNT.

$$\begin{Bmatrix}\sigma_{11}\\ \sigma_{22}\\ \sigma_{33}\\ \sigma_{23}\\ \sigma_{13}\\ \sigma_{12}\end{Bmatrix}=C\begin{Bmatrix}\varepsilon_{11}\\ \varepsilon_{22}\\ \varepsilon_{33}\\ \varepsilon_{23}\\ \varepsilon_{13}\\ \varepsilon_{12}\end{Bmatrix},\qquad C=\begin{bmatrix}k+m & l & k-m & 0 & 0 & 0\\ l & n & l & 0 & 0 & 0\\ k-m & l & k+m & 0 & 0 & 0\\ 0 & 0 & 0 & p & 0 & 0\\ 0 & 0 & 0 & 0 & m & 0\\ 0 & 0 & 0 & 0 & 0 & p\end{bmatrix} \tag{1}$$

where *k, l, m, n,* and *p* are Hill's elastic moduli; *k* is the plane-strain bulk modulus normal to the fiber direction, *n* is the uniaxial tension modulus in the fiber direction (x_2), *l* is the associated cross modulus, *m* and *p* are the shear moduli in normal and parallel planes to the fiber direction, respectively. These are expressed mathematically as follows [24]:

$$l=\frac{E_m\left\{c_m\nu_m[E_m+2k_r(1+\nu_m)]+2c_rl_r(1-\nu_m{}^2)\right\}}{(1+\nu_m)[2c_mk_r(1-\nu_m-2\nu_m{}^2)+E_m(1+c_r-2\nu_m)]} \tag{2a}$$

$$k=\frac{E_m\left\{E_mc_m+2k_r(1+\nu_m)[1+c_r(1-2\nu_m)]\right\}}{2(1+\nu_m)[E_m(1+c_r-2\nu_m)+2c_mk_r(1-\nu_m-2\nu_m{}^2)]} \tag{2b}$$

$$p=\frac{E_m[E_mc_m+2(1+c_r)p_r(1+\nu_m)]}{2(1+\nu_m)[E_m(1+c_r)+2c_mp_r(1+\nu_m)]} \tag{2c}$$

$$m=\frac{E_m[E_mc_m+2m_r(1+\nu_m)(3+c_r-4\nu_m)]}{2(1+\nu_m)\{E_m[c_m+4c_r(1-\nu_m)]+2c_mm_r(3-\nu_m-\nu_m{}^2)\}} \tag{2d}$$

$$n=\frac{E_m{}^2c_m(1+c_r-c_m\nu_m)+c_mc_r(k_rn_r-l_r{}^2)(1+\nu_m)^2(1-2\nu_m)}{(1+\nu_m)\{2c_mk_r(1-\nu_m-2\nu_m{}^2)+E_m(1+c_r-2\nu_m)\}}+\frac{E_m[2c_m{}^2k_r(1-\nu_m)+c_rn_r(1-2\nu_m+c_r)-4c_ml_r\nu_m)]}{2c_mk_r(1-\nu_m-2\nu_m{}^2)+E_m(1-2\nu_m+c_r)} \tag{2e}$$

where E_m and υ_m are Young's modulus and Poisson's ratio, respectively, and k_r, l_r, m_r, n_r, and p_r are the Hill's elastic moduli for the reinforcing phase (CNTs). For polystyrene $E_m=1.9\,\text{Gpa}$ and $\upsilon_m=0.3$ and Hill's elastic moduli of SWCNTs with $10\,A°$ and $20\,A°$ radii are listed in Table 1 [23, 25].

2.1 Thermal analysis

Consider a thick-walled FG polystyrene nanocomposite cylinder with infinite length as illustrated in Fig. 2. Straight SWCNTs are embedded along the axial direction of the cylinder. Assuming cylindrical coordinate system (r, θ, z), and the volume fraction of the constituent (c) for both the reinforced CNT material and the matrix are c_r and c_m, then [14]:

$$c_r+c_m=1 \tag{3}$$

As can be seen from Fig. 3a, when the volume fraction of SWCNTs is uniformly distributed (UD), c_r is defined as follow:

$$c_r=V_{CN}{}^* \tag{4}$$

where $V_{CN}{}^*=\dfrac{w_{CN}}{w_{CN}+(\rho_{CN}/\rho_m)-(\rho_{CN}/\rho_m)w_{CN}}$ [14] and w_{CN} is the mass fraction of the SWCNTs, ρ_m and ρ_{CN} are densities of matrix and carbon nanotubes, respectively, and $V_{CN}{}^*$ specific volume fraction of carbon nanotube.

Table 1
Hill's elastic moduli of reinforced CNTs [23,25]

CNT Radius (A^o)	k_r(Gpa)	l_r(Gpa)	m_r(Gpa)	n_r(Gpa)	p_r(Gpa)
10	30	10	1	450	1
20	4	2	0.1	250	0.1

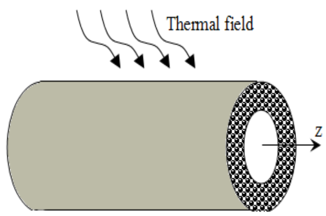

Fig. 2
Configuration of thick-walled cylinder embedded with SWCNTs under thermal field.

With respect to FG material, two types of variations (or layouts) in the volume fraction of SWCNTs were considered in the structure of the FG cylinder along the radius from inner to outer surface, namely: incrementally decreasing (Inc Dec) and incrementally increasing (Inc Inc) (see Fig. 3b). The former refers to the structure in which the volume fraction of the SWCNTs is reduced from inner to outer surface, while for the latter, this is increased c_r for both Inc Dec and Inc Inc are as explained below in Eqs. (5) and (6), respectively:

$$c_r = \left(1 + 2\frac{1-\zeta}{1-h}\right) V_{CN}{}^{*} \tag{5}$$

$$c_r = \left(1 + 2\frac{\zeta - h}{1-h}\right) V_{CN}{}^{*} \tag{6}$$

where ζ and h are the dimensionless radius and ratio of the inner to outer radius of the cylinder or aspect ratios, respectively, i.e.

$$\zeta = r / r_o , \qquad h = r_i / r_o \tag{7}$$

The physical properties for polystyrene and SWCNTs are as follows [14, 26]: $\rho_m = 1.05(\text{kg/m}^3)$, $\rho_{CN} = 1.4(\text{kg/m}^3)$, $w_{CN} = 0.13$, and $V_{CN}{}^{*} = 0.11$. The general equations of motion and strain-displacement relations for a thick-walled cylinder could be written as [18]:

$$\begin{aligned}
&\frac{\partial \sigma_{rr}}{\partial r} + \frac{1}{r}\frac{\partial \sigma_{r\theta}}{\partial \theta} + \frac{\partial \sigma_{rz}}{\partial z} + \frac{\sigma_{rr} - \sigma_{\theta\theta}}{r} + F_r = \rho \frac{\partial^2 u_r}{\partial t^2} \\
&\frac{\partial \sigma_{\theta r}}{\partial r} + \frac{1}{r}\frac{\partial \sigma_{\theta\theta}}{\partial \theta} + \frac{\partial \sigma_{\theta z}}{\partial z} + \frac{2\sigma_{\theta r}}{r} + F_\theta = \rho \frac{\partial^2 u_\theta}{\partial t^2} \\
&\frac{\partial \sigma_{zr}}{\partial r} + \frac{1}{r}\frac{\partial \sigma_{z\theta}}{\partial \theta} + \frac{\partial \sigma_{zz}}{\partial z} + \frac{\sigma_{zr}}{r} + F_z = \rho \frac{\partial^2 u_z}{\partial t^2}
\end{aligned} \tag{8}$$

$$\begin{aligned}
&\varepsilon_{rr} = \frac{\partial u_r}{\partial r}, \qquad \varepsilon_{\theta\theta} = \frac{1}{r}\frac{\partial u_\theta}{\partial \theta} + \frac{u_r}{r}, \qquad \varepsilon_{zz} = \frac{\partial u_z}{\partial z} \\
&\varepsilon_{r\theta} = \frac{1}{2}\left(\frac{\partial u_\theta}{\partial r} + \frac{1}{r}\frac{\partial u_r}{\partial \theta} - \frac{u_\theta}{r}\right), \qquad \varepsilon_{\theta z} = \frac{1}{2}\left(\frac{\partial u_\theta}{\partial z} + \frac{1}{r}\frac{\partial u_z}{\partial \theta}\right), \qquad \varepsilon_{rz} = \frac{1}{2}\left(\frac{\partial u_z}{\partial r} + \frac{\partial u_r}{\partial z}\right)
\end{aligned} \tag{9}$$

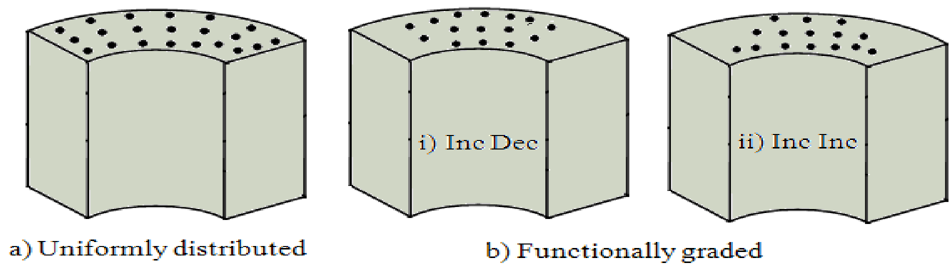

Fig. 3
Variations in the volume fraction of SWCNTs considered: a) Uniformly distributed b) functionally graded *i*) Inc Dec, *ii*) Inc Inc.

When the nanocomposite cylinder is subjected to a thermal field, thermal strains are created in three directions in the stress-strain relations as in Eq. (10) as follows [18]:

$$\begin{Bmatrix}\sigma_r\\ \sigma_z\\ \sigma_\theta\\ \sigma_{\theta z}\\ \sigma_{zr}\\ \sigma_{r\theta}\end{Bmatrix}=C\begin{Bmatrix}\varepsilon_r-\lambda_r T\\ \varepsilon_z-\lambda_z T\\ \varepsilon_\theta-\lambda_\theta T\\ 2\gamma_{\theta z}\\ 2\gamma_{zr}\\ 2\gamma_{r\theta}\end{Bmatrix},\quad C=\begin{bmatrix}k+m & l & k-m & 0 & 0 & 0\\ l & n & l & 0 & 0 & 0\\ k-m & l & k+m & 0 & 0 & 0\\ 0 & 0 & 0 & p & 0 & 0\\ 0 & 0 & 0 & 0 & m & 0\\ 0 & 0 & 0 & 0 & 0 & p\end{bmatrix} \tag{10}$$

where λ is the thermal modulus, T denotes the temperature expressed in absolute unit. In Eq. (10), elastic modulus and thermal expansion coefficients are related as follows [18]:

$$\begin{cases}\lambda_r=C_{11}\alpha_r+C_{12}\alpha_z+C_{13}\alpha_\theta\\ \lambda_z=C_{21}\alpha_r+C_{22}\alpha_z+C_{23}\alpha_\theta\\ \lambda_\theta=C_{31}\alpha_r+C_{32}\alpha_z+C_{33}\alpha_\theta\end{cases}\quad \begin{cases}C_{11}=k+m\\ C_{12}=l\\ C_{11}=k-m\end{cases} \tag{11}$$

Based on Mori-Tanaka method, nanocomposite characteristics are assumed to be transversely isotropic which can only be applied where SWCNTs are uniformly distributed. This is because the nanocomposite characteristics are orthotropic for FG materials. Despite this, assuming the structure is almost uniform and c_r changes slightly and linearly in such a way that properties do not alter significantly in radial and circumferential directions, one might employ the introduced stiffness matrix in Eq. (1) for FG materials.

The thermal expansion coefficients of nanocomposite in z, r and θ directions may be written as:

$$\alpha_z=c_r\alpha_z^{CN}+c_m\alpha^m \tag{12a}$$

$$\alpha_r=(1+\nu_z^{CN})c_r\alpha_r^{CN}+(1+\nu^m)c_m\alpha^m-\nu_\zeta\times\alpha_z \tag{12b}$$

$$\alpha_r=\alpha_\theta \tag{12c}$$

$$\nu_\zeta=c_r\nu_z^{CN}+c_m\nu^m \tag{13}$$

where α_r^{CN}, α_z^{CN} are thermal expansion coefficients of SWCNTs in longitudinal and radial directions, respectively, and α^m is the thermal expansion coefficient of the matrix assumed to be $\alpha^m=7\times10^{-5}(\mathrm{K}^{-1})$ [26]. However,

α_r^{CN}, α_z^{CN} are not expected to alter significantly for the temperature range of 300 K<T<700 K considered in this work. Hence, their average values are taken at 500K from the data used by [14] as expressed in Table 2. Also, in the above equations, υ_z^{CN}, υ_m are Poisson's ratios SWCNTs and matrix assumed to be $\upsilon_z^{CN} = 0.175$, $\upsilon_m = 0.3$ [14, 23].

For practical purposes, stress, strain and thermal moduli can be rewritten in dimensionless form of as follows:

$$\theta = \frac{T}{T_0}, \qquad \varepsilon_\theta = \alpha_r T_0 \frac{u_0}{\zeta}, \qquad \varepsilon_r = \alpha_r T_0 \frac{\partial u_0}{\partial \zeta}, \qquad u_0 = \frac{u}{\alpha_r T_0 b}$$

$$\Lambda_i = \frac{\lambda_{ii}}{C_{11}\alpha_r} \ (i = r, z, \theta), \qquad \sigma_i = \frac{\sigma_{ii}}{\alpha_r T_0 C_{11}} \ (i = r, z, \theta) \tag{14}$$

2.2 Analytical solution

For the cylinder studied in this work, the following assumptions may be considered: the cylinder in static equilibrium, plane strain $(\varepsilon_z = 0)$, $u(\theta) = 0$ and $u_r = u(r)$. Using Eqs. (8), (9) and (10), the following ordinary second order differential equation is obtained:

$$u_0'' + \frac{u_0'}{\zeta} - \frac{u_0}{\zeta^2} - \left(\frac{\partial \Lambda_r}{\partial \zeta}\theta + \Lambda_r \frac{\partial \theta}{\partial \zeta} \right) = 0 \tag{15}$$

The boundary conditions are defined as:

$$\sigma_r(h) = 0, \qquad \sigma_r(1) = 0 \tag{16}$$

In order to solve Eq. (16), the temperature distribution should be determined. The general form of the governing equation of heat conduction in cylindrical coordinates can be written as [27]:

$$k\left(\frac{\partial^2 T}{\partial r^2} + \frac{1}{r}\frac{\partial T}{\partial r} + \frac{1}{r^2}\frac{\partial^2 T}{\partial \varphi^2} + \frac{\partial^2 T}{\partial z^2} \right) + R = \rho c \frac{\partial T}{\partial t} \tag{17}$$

where k, R, and c are conductivity, rate of heat generation and specific thermal capacity, respectively. Assuming infinite length for the cylinder, no internal heat generation, steady state thermal field and axisymmetrical temperature distribution (i.e. $\partial^2 T / \partial \varphi^2 = 0$, $\partial^2 T / \partial z^2 = 0$), the heat transfer equation is simplified to:

$$\left(\frac{\partial^2 T}{\partial r^2} + \frac{1}{r}\frac{\partial T}{\partial r} \right) = 0 \tag{18}$$

For dimensionless form, Eq. (18) is expressed as:

Table 2
Temperature-dependent thermal expansion coefficients of SWCNTs in the longitudinal and radial directions [14]

Temperature (K)	$\alpha_Z^{CN} (\times 10^{-6} / \mathrm{K})$	$\alpha_r^{CN} (\times 10^{-6} / \mathrm{K})$
300	3.4584	5.1682
500	4.5361	5.0189
700	4.6677	4.8943

$$\left(\frac{\partial^2\theta}{\partial\zeta^2}+\frac{1}{\zeta}\frac{\partial\theta}{\partial\zeta}\right)=0 \tag{19}$$

Assuming temperature at both inner and outer surfaces of the cylinder remains constant as T=300 K and T_o=500 K, respectively, with the surrounding temperature of T_0=300 K, the temperature profile is written in the following form:

$$\theta = A + B\ln\zeta \tag{20}$$

Considering boundary conditions Eq. (16), the temperature profile becomes:

$$\theta=\frac{1}{T_0\ln(h)}\times\left[\left(T_i-T_o\right)\ln\zeta+T_o\times\ln h\right] \tag{21}$$

Substituting Eq. (21) in Eq. (15) yields the displacement u_0 as follows:

$$f(\zeta)=\left(\frac{\partial\Lambda_r}{\partial\zeta}\theta+\Lambda_r\frac{\partial\theta}{\partial\zeta}\right) \tag{22}$$

$$\frac{\partial}{\partial\zeta}\left[\frac{1}{\zeta}\frac{\partial}{\partial\zeta}(\zeta u_0)\right]=f(\zeta) \tag{23}$$

$$u_0(\zeta)=C_1+C_2\zeta^{-1}+\zeta^{-1}\int_0^{\zeta}\zeta\left[\int_0^{\zeta}f(\zeta)\mathrm{d}\zeta\right]\mathrm{d}\zeta \tag{24}$$

Stress distribution in various directions may be obtained by substituting Eq. (24) into Eqs. (9) and (10).

3 NUMERICAL RESULTS AND DISCUSSION

In this section, numerical results obtained using core relations. Figs. 4 demonstrate dimensionless displacement across thickness of the cylinder for different layouts at aspect ratios $(h = r_i / r_o)$ of 0.2, 0.4, and 0.6, 0.8 in Fig. 4a and Fig. 4b, respectively. Larger aspect ratio corresponds to smaller and thinner cylinders. As can be seen, dimensionless displacement changes almost linearly with dimensionless radius and the rate of this change is less for higher aspect ratios h. Also, maximum displacement takes place at the outer surface of cylinder and for all aspect ratios considered here, Inc-Inc layout shows the least displacement, compared with Inc-Dec and UD.

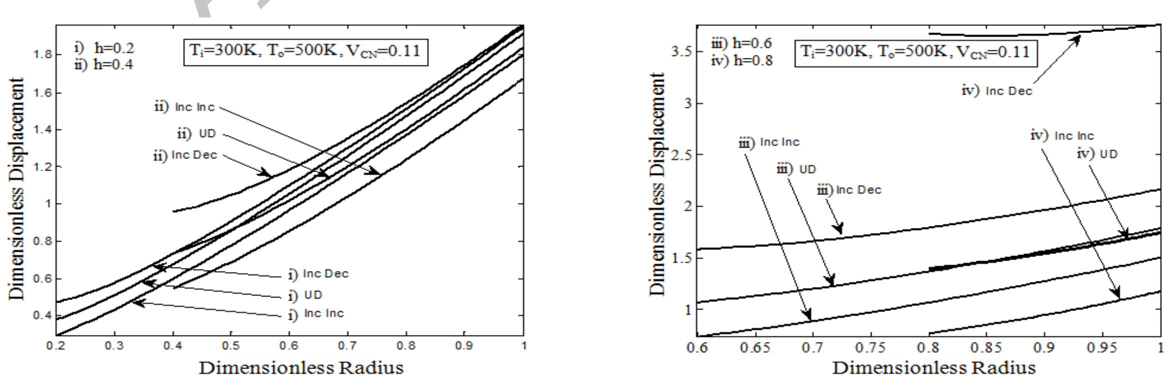

(a) (b)

Fig. 4
Distribution of dimensionless displacement versus dimensionless radius.

The difference between Inc-Inc and Inc-Dec for the same *h* becomes more apparent for higher aspect ratios. As far as bonding between CNT and the matrix is concerned, for constant volume fraction of CNT which is the case in this study, as *h* is increased, displacement and consequently interface debonding between matrix and CNT are increased. Figs. 5 show distribution of dimensionless radial stress across thickness of the cylinder for various layouts and aspect ratios as above. As can be seen, maximum stress takes place near the inner surface of the cylinder for low *h* and decreases with increasing *h*. For all aspect ratios considered here, Inc-Inc layout shows the least dimensionless radial stress, compared with Inc-Dec and UD. Figs. 6 depict distribution of dimensionless circumferential stress across thickness of the cylinder for various layouts and aspect ratios. Maximum tensional circumferential stress takes place at the inner surface of the cylinder. Circumferential stress increases with increasing *h* irrespective of the layout type. The same as radial stress in Figs. 5, for all aspect ratios, Inc-Inc layout shows the least dimensionless circumferential stress, compared with Inc-Dec and UD. Fig.7 show circumferential stress distribution across thickness of the cylinder in *h*=0.2 for two radius of SWCNTs. It is observed from this figure that when radius of CNTs is increased, the circumferential stress in Inc-Dec layout increases; while for Inc-Inc, the riverse is true. Also, increasing radius of CNTs does not seem to affect significantly dimensionless circumferential stress in UD layout. Circumferential stress decreases with increasing ζ for all radii and layouts of CNTs.

Fig. 8 shows the distribution of von-Mises stress across thickness of the cylinder in *h*=0.4 for various layouts. The plots of axial stresses, σ_z versus the dimensionless radius has not been presented here for brevity. As can be seen, the von-Mises stress has increased almost linearly with the dimensionless radius for both cases of Inc Inc and UD layouts with the former having a higher gradient. Also, minimum von-Mises stress happens for UD layout and it is therefore, recommended for the optimum design of nanocomposite thick-walled cylindrical vessels.

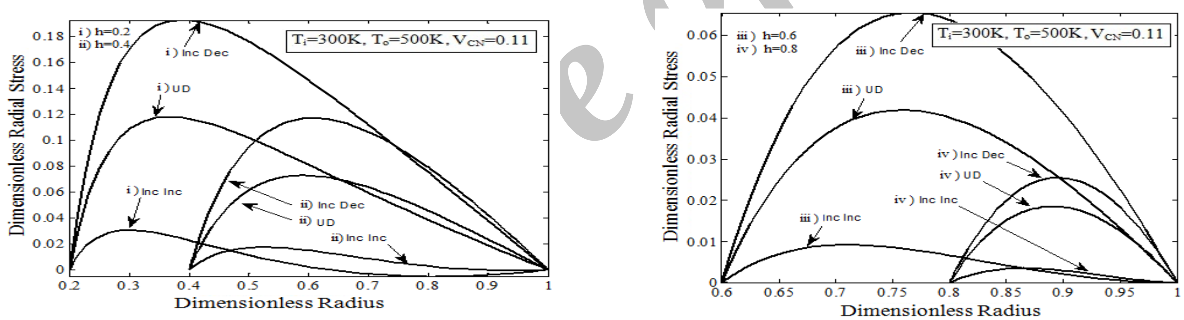

(a) (b)

Fig. 5
Distribution of dimensionless radial stress versus dimensionless radius.

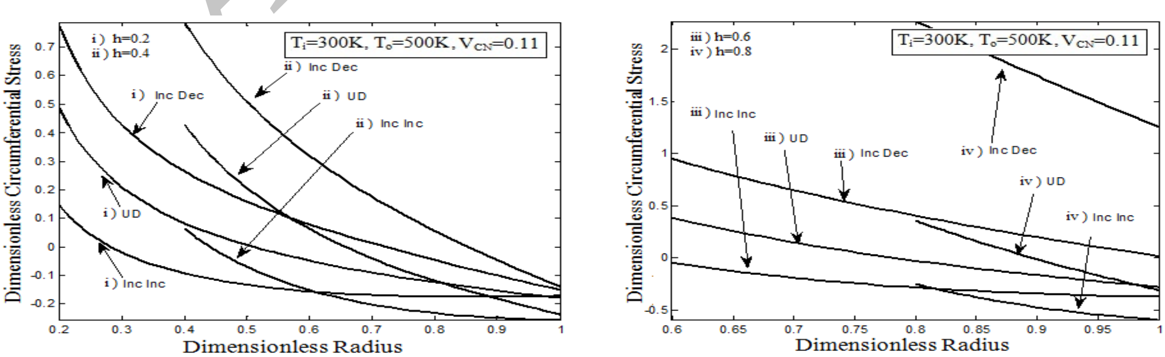

(a) (b)

Fig. 6
Distribution of dimensionless circumferential stress versus dimensionless radius.

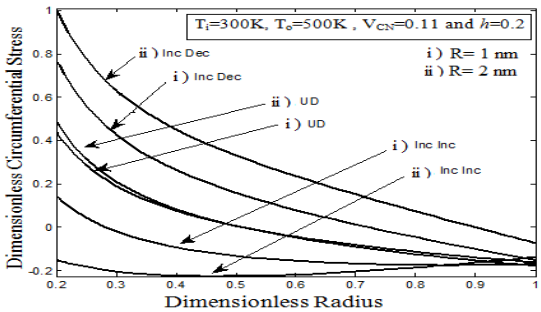

Fig. 7
Distribution of dimensionless circumferential stress versus dimensionless radius.

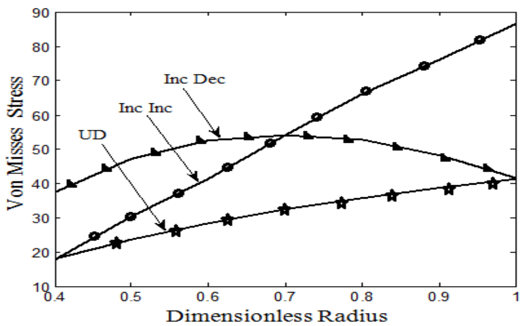

Fig.8
Distribution of dimensionless von-Mises stress versus dimensionless radius.

4 CONCLUSIONS REMARKS

Thermal stresses and displacement analysis of a thick-walled cylinder reinforced by FG SWCNTs in radial direction has been presented. Nanocomposite cylinder is subjected to a steady state thermal field. The SWCNTs are assumed aligned, straight with infinite length and a uniform layout. Two layouts of variations in the volume fraction of SWCNTs were considered in the structure of the FG cylinder along the radius from inner to outer surface, namely Inc Inc and Inc Dec. These are compared with UD structure. Mori-Tanaka method is employed for stress-strain analysis. Using equations of motion, stress-strain and their corresponding constitutive correlations of a polystyrene vessel, a second order ordinary differential equation is proposed based on radial displacement. This is then solved in order to obtain the distribution of displacement and radial, circumferential and axial stresses. For constant temperatures at the inner and outer surfaces of the FG cylinder considered here, results in this work indicate that radial and circumferential stresses and displacement are lower for the Inc Inc FG cylinder, and the axial stresses are higher irrespective of the structure of the FG material.

1) Furthermore, increasing the aspect ratios has reduced radial stress in all layouts.
2) Circumferential stress for UD and Inc Inc cylinders and has increased it for Inc Dec cylinder.

As far as variations of the SWCNTs radius is concerned, increasing this

a) Has reduced radial and circumferential stresses in Inc Inc cylinder
b) Has increased radial and circumferential stresses in Inc Dec cylinder

The corresponding analyses of axial sresses have not been presented here for brevity of results. However, results on von Mises stress show that it has increased almost linearly with the dimensionless radius for both cases of Inc Inc and UD layouts. UD layout is recommended for optimum design of nanocomposite thick-walled cylindrical vessels as minimum von-Mises stress takes place in it.

ACKNOWLEDGEMENTS

The authors would like to thank the referees for their valuable comments. The authors are also grateful to University of Kashan for supporting this work by Grant No. 65475/16.

REFERENCES

[1] Saito R., Dresselhaus G., Dresselhaus M.S., 1998, *Physical Properties of Carbon Nanotubes*, Imperial College Press, London.

[2] Qian D., Wagner G.J., Liu W.K., Yu M.F., Ruoff R.S., 2002, Mechanics of Carbon Nanotubes, *Applied Mechanics Reviews* **55**(6): 495-533.

[3] Ajayan P.M., Stephan O., Colliex C., Trauth D., 1994, Aligned carbon nanotube arrays formed by cutting a polymer resin—nanotube composite, *Science* **256**: 1212-1214.

[4] Lourie O., Cox D.M., Wagner H.D., 1998, Buckling and Collapse of Embedded Carbon Nanotube, *Physical Review Letters* **81**(8): 1638-1641.

[5] Haggenmueller R., Gommans H.H., Rinzler A.G., Fischer J.E., Winey K.I., 2000, Aligned Single-Wall Carbon Nanotubes In Composites by Melt Processing Methods, *Chemical Physics Letters* **330**: 219-225.

[6] Fidelus J.D., Wiesel E., Gojny F.H., Schulte K.,Wagner H.D., 2005, Thermo-mechanical properties of randomly oriented Carbon/epoxy nanocomposites, *Composites Part A: Applied Science and Manufacturing* **36**: 1555-1361.

[7] Bonnet P., Sireude D., Garnier B., Chauvet O., 2007, Thermal properties and percolation in carbon nanotube–polymer composites, *Journal of Applied Physics* **91**: 201910.

[8] Qian D., Dickey E.C., Andrews R., Rantell T., 2000, Load Transferand and Deformation Mechanisms in Carbon Nanotube-Polystyrene Composites, *Applied Physics Letters* **76**: 2868-2870.

[9] Odegard G.M., Gates T.S., Wise K.E., Park C., Siochi E.J., 2002, Constitutive Modeling of Nanotube-Reinforced Polymer Composites, *Composites Science and Technology* **63**(11): 1671-1687.

[10] Wuite J., Adali S., 2005, Deflection and stress behaviour of nanocomposite reinforced beams using a multiscale analysis, *Composite Structures* **71**: 388-396.

[11] Vodenitcharova T., Zhang L.C., 2006, Bending and local buckling of a nanocomposite beam reinforced by a single-walled carbon nanotube, *International Journal of Solids and Structures* **43**: 3006-3024.

[12] Han Y., Elliott J., 2007, Molecular dynamics simulations of the elastic properties of polymer/ carbon nanotube composites, *Computation Materials Science* **39**: 315-323.

[13] Zhu R., Pan E., Roy A.K., 2007, Molecular dynamics study of the stress-strain behavior of carbon-nanotube reinforced Epon 862 composites, *Materials Science and Engineering A* **447**: 51-57.

[14] Shen H.S., 2009, Nonlinear bending of functionally graded carbon nanotubereinforced composite plates in thermal environments, *Composite Structures* **91**: 9-19.

[15] Ke L.L., Yang J., Kitipornchai S., 2010, Nonlinear free vibration of functionally graded carbon nanotube-reinforced composite beams*,* *Composite Structures* **92**(3): 676-683.

[16] Wang X., 1995, Thermal shock in a hollow cylinder caused by rapid arbitrary heating, *Journal of Sound and Vibration* **183**: 899-906.

[17] Cho H., Kardomateas G.A., Valle C.S.,1998, Elastodynamic solution for the thermal shock stresses in an orthotropic thick cylindrical shell*,* *Journal of Applied Mechanics* **65**: 184-192.

[18] Ding H.J., Wang H.M., Chen W.Q., 2001, A theoretical solution of cylindrically isotropic cylindrical tube for axisymmetric plane strain dynamic thermoelastic problem, *Acta Mechanica Solida Sinica* **14**: 357-363.

[19] Pelletier J.L., Vel S.S., 2006, An exact solution for the steady-state thermoelastic response of functionally graded orthotropic cylindrical shells, *International Journal of Solids and Structures* **43**: 1131-1158.

[20] Horgan C.O., Chan A.M., 1999, the pressurized hollow cylinder or disk problem for functionally graded isotropic linearly elastic materials, *Journal of Elasticity* **55**: 43-59.

[21] Tarn J.Q., 2001, Exact solutions for functionally graded anisotropic cylinders subjected to thermal and mechanical loads. *International Journal of Solids and Structures* **38**: 8189-8206.

[22] Abd-Alla A.M., Farhan A.M., 2008, Effect of the non-homogenity on the composite infinite cylinder of orthotropic material, *Physics Letters A* **372**: 756-260.

[23] Shi D.L., Feng X.Q., Huang Y.Y., Hwang K.C., Gao H., 2004, The effect of nanotube waviness and agglomeration on the elastic property of carbon nanotube-reinforced composites, *Journal of Engineering Materials and Technology* **126**: 250-257.

[24] Hill R., 1965, A Self- Consistent Mechanics of Composite Materials, *Journal of the Mechanics and Physics of Solids* **13**: 213-222.

[25] Popov V.N., Van Doren V.E., Balkanski M., 2000, Elastic Properties of Crystals of Single-Walled Carbon Nanotubes, *Solid State Communications* **114**: 395–399.

[26] Mark J.E., 1999, *Polymer Data Handbook*, Oxford University Press, New York. Oxford.

[27] Hetnarski R.B., Eslami M.R., 2008, *Thermal Stresses Advanced Theory and Application*, Springer.